Support Information for

Reference-free Quantitative Mass Spectrometry in the Presence of Nonlinear

Distortion Caused by In-Situ Chemical Reactions among Constituents

Yusuke Hibi*

Data-driven Polymer Design Group, Research Center for Macromolecules and Biomaterials, National Institute for Materials Science (NIMS); 1-2-1, Sengen, Tsukuba, Ibaraki 305-0047, Japan.

*Corresponding authors. Emails: hibi.yusuke@nims.go.jp

This PDF file includes:

Methods

Supplementary Figure S1-S5

Supplementary Tables S1-2

Captions for Data S1

Reference list cited in this support information file.

Other Supplementary Materials for this manuscript include the following:

The raw spectra and sample information are available at *Analyst*, **2024**, DOI: 10.1039/D4AN00624K (Data S3, Gly-Jeff-Silox dataset). The ready-to-use starting matrix obtained by processing this raw data is attached to this manuscript as Data S1.

Methods

<u>Mathematical notations</u>

The notation largely adheres to the standard conventions used in signal processing. The symbols $\mathbb{R}_+^{N \times M}$ and $\mathbb{R}^{N \times M}$ denote a non-negative real matrix and a real matrix, respectively, each with dimensions $N \times M$. For a matrix $X \in \mathbb{R}^{N \times M}$, $X_{n:} \in \mathbb{R}^{1 \times M}$, $X_{:m} \in \mathbb{R}^{N \times 1}$, $X_{nm} \in \mathbb{R}$ represent the nth row vector, m^{th} column vector, and (n, m)-element of the matrix X, respectively. The notation X^T stands for the transpose of matrix X. The Frobenius norm of X is indicated by $\|X\|_F$. The symbols of $\|X_{n:}\|_1$ and $\|X_{n:}\|_2$ represent the ℓ_1- and ℓ_2-norm of nth row vector of X, respectively. For a square matrix of X, $Tr(X)$ represents its trance. $\mathbf{1}_N$, $\mathbf{11}_N$ and I_N stand for a N-dimensional all-ones vector, (N, N)-dimensional all-ones matrix and N-dimensional identity matrix, respectively.

<u>Preparation of the starting matrix A representing fragment abundance (FA) (Fig. 2A)</u>

The ready-to-use spectral dataset of the Gly-Jeff-Silox system is available in the previous report.[1] The dataset X contained 310 spectra (31 samples $\times$ 10 temperature bands from 300 to 600 °C) with 2537 channels. Therefore, X was a matrix with the size of (310, 2537), which was subjected to the reported NMF algorithm: $X \approx AS$, where $S \in \mathbb{R}_+^{M \times D}$ represents 27–fragment spectra (Fig. S1) and $A \in \mathbb{R}_+^{10N \times M}$ represents their abundances in each sample (Fig. 2A), where $N = 31$, $M = 27$ and $D = 2537$. Note that A originally represented a spectrum-wise FA with a dimension of (310, 27), which was converted into a sample-wise FA with a dimension of (31, 27), which was further converted into weight fraction using synchronized thermogravimetry data as previously described.[1] The NMF

hyperparameter was the same as previous report and presented in Table S1.

The conventional linear RQMS performs two step NMF: $X \approx AS \approx (CB)S$, as described in the main text.[2] NL-RQMS aims to achieve better compositional analysis for interactive/reactive systems by introducing a bilinear model in the second factorization step yet starting with the same matrix A as in conventional RQMS. The starting matrix A with size of (N, M) can be found in attached Data S1.

Quick review of linear RQMS

The first NMF $X \approx AS$ extracts the most representative M–fragment spectra S and their abundances (FA) in each sample A. The second NMF $A \approx CB$ finds the FA of K–pure constituents $B \in \mathbb{R}_+^{K \times M}$ and their concentration in each sample $C \in \mathbb{R}_+^{N \times K}$. The second NMF uses so-called volume minimization algorithm (VolMin),[3] which finds the volume-minimized simplex spanned by the rows of B and enclosing all the rows of A. This can be formulated as follows:

$$\min_{C,B} \frac{1}{2} \|A - CB\|_F^2 + vol(B) \tag{1}$$

$$s.t. \, B \geq 0, C \geq 0, C1_K = 1_N.$$

The first term is of approximation residuals and the second term is of the volume regularization of the simplex. However, this cannot output accurate composition because $A_{n:}$ represents the coordinates of nth sample in the non-orthogonal coordinate system spanned by S. To consider this non-orthogonality originating from the first NMF, the approximation residuals $D(A|CB)$ should be evaluated in Riemann metrics, i.e.:

$$D(A|CB) = Tr[(A - CB)SS^T(A - CB)^T].$$

The significance of using Riemann metrics is that the distance between A and CB can be evaluated in the original spectral space, as depicted in Fig. 3. Using a lower triangular matrix $L \in \mathbb{R}^{M \times M}$ obtained via Cholesky decomposition of SS^T, the residuals can be written as follows:

$$D(A|CB) = Tr[(A - CB)LL^T(A - CB)^T] = \left\|\widehat{A} - C\widehat{B}\right\|_F^2,$$

where $\widehat{A} = AL \in \mathbb{R}^{N \times M}$ and $\widehat{B} = BL \in \mathbb{R}^{K \times M}$. The equation (1) then becomes as follows with additional orthogonal constraints:

$$\min_{C, \widehat{B}} \frac{1}{2} \left\|\widehat{A} - C\widehat{B}\right\|_F^2 + \frac{\alpha}{2} vol(\widehat{B}) + \frac{\beta}{2} nonorth(\widehat{B}), \qquad (2)$$

$$s.t. \widehat{B} = BL, B \geq 0, C \geq 0, C1_K = 1_N,$$

where $nonorth(\widehat{B})$ is a non-orthogonality term of row vectors of $\widehat{B}$, and $\alpha > 0, 1 > \beta > 0$ are regularization parameters controls volume-shrinking and volume-expanding force applied to the simplex. Although the selection of hyperparameters influence the final compositional results, 0.1 for both α and β were consistently used and gave sufficiently accurate results in the previous reports. These regularization terms were formulated as follows:

$$vol(\widehat{B}) = \log\left|\det\left(\widehat{B}\widehat{B}^T + \tau I_K\right)\right|,$$

$$nonorth(\widehat{B}) = Tr\left(\Lambda\left(\widehat{B}\widehat{B}^T - diag\left(\widehat{B}\widehat{B}^T\right)\right)\right),$$

where $\Lambda \in \mathbb{R}^{K \times K}$ is a symmetric Lagrange multiplier matrix. The equation (2) cannot be solved directly since both C and $\widehat{B}$ are unknown. Therefore, they were alternatively and

iteratively updated starting from the initial C and $\widehat{B}$ set by vertex component analysis. At the tth update, the update to $C^{(t+1)}$ can be achieved using a simple algorithm of non-negative least square (NNLS)[4] based on temporal $\widehat{B}^{(t)}$, here denoted as $C^{(t+1)} = NNLS(\widehat{A}; \widehat{B}^{(t)})$. On the other hand, updating rule for $\widehat{B}$ is much more complicated due to the regularization terms and non-negative restriction; yet it can be updated based on $\widehat{A}$ and $C^{(t)}$ as derived in the previous report, and here denotation of $\widehat{B}^{(t+1)} = volmin(\widehat{A}; C^{(t)})$.

Mathematical derivation of the NL-RQMS

For analyzing interactive systems, the nonlinear correction term should be incorporated in the second factorization,[5] i.e.:

$$A \approx CB + C'B', \tag{3}$$

where $B'_{k:}$ $(k = 1, 2, \dots K')$ represents the kth cross-component of (l, m)-components, $K' = \binom{K}{2}$, and (l, m) is the index combination of two-combination of K. The kth column of C' is calculated by pairwise multiplication of the columns of C:

$$C'_{:k} = C_{:l} \odot C_{:m}, for \ k = 1, 2, \dots K', \tag{4}$$

where $\odot$ represents element-wise production.

As described above, the approximation residual should be evaluated using Riemann metrics. The equation (3) becomes $\widehat{A} \approx C\widehat{B} + C'\widehat{B'}$ where $\widehat{A} = AL, \widehat{B} = BL, \widehat{B'} = B'L$. As the vertices of pure component spectra are consistent regardless of the existence of interactions, the same regularization terms for $\widehat{B}$ were applied as (2). The NL-RQMS algorithm then can be formulated as follows:

$$\min_{\boldsymbol{C},\widehat{\boldsymbol{B}},\widehat{\boldsymbol{B}}'} \frac{1}{2}\left\|\widehat{\boldsymbol{A}} - \boldsymbol{C}\widehat{\boldsymbol{B}} - \boldsymbol{C}'\widehat{\boldsymbol{B}}'\right\|_F^2 + \frac{\alpha}{2}vol(\widehat{\boldsymbol{B}}) + \frac{\beta}{2}nonorth(\widehat{\boldsymbol{B}}) + \rho\|\boldsymbol{B}'\|_1, \qquad (5)$$

$$s.t. \widehat{\boldsymbol{B}} = \boldsymbol{BL}, \widehat{\boldsymbol{B}'} = \boldsymbol{B}'\boldsymbol{L}, \boldsymbol{B} \geq 0, \boldsymbol{C} \geq 0, \boldsymbol{C}\boldsymbol{1}_K = \boldsymbol{1}_N,$$

where $\boldsymbol{C}'$ can be calculated from $\boldsymbol{C}$ according to equation (4). The regularization term of $\rho\|\boldsymbol{B}'\|_1$ express the chemical knowledge that the polymer substructures involved in reaction/interaction should be limited, and the hyperparameter ρ controls the nonlinearity of the model. Introducing $\widehat{\boldsymbol{A}}' \equiv \widehat{\boldsymbol{A}} - \boldsymbol{C}'\widehat{\boldsymbol{B}'}$ makes the problem (5) become very similar to problem (2). If $\widehat{\boldsymbol{B}'}^{(t)}$ is given at t^{th} iteration, $\widehat{\boldsymbol{B}}^{(t+1)}$ can be updated using exact same algorithm: $\widehat{\boldsymbol{B}}^{(t+1)} = volmin(\widehat{\boldsymbol{A}'}^{(t)}; \boldsymbol{C}^{(t)})$. However, the update rule of $\boldsymbol{C}^{(t+1)}$ should be modified from the simple NNLS, because this update affects $\boldsymbol{C}'$ as well.

To consider the update rule for $\boldsymbol{C}$, the objective function is defined as follows: $L \equiv \frac{1}{2}\left\|\widehat{\boldsymbol{A}} - \boldsymbol{C}\widehat{\boldsymbol{B}} - \boldsymbol{C}'\widehat{\boldsymbol{B}'}\right\|_F^2 = \frac{1}{2}\left\|\widehat{\boldsymbol{A}} - \widetilde{\boldsymbol{C}}\widetilde{\boldsymbol{B}}\right\|_F^2$, where $\widetilde{\boldsymbol{B}} \equiv \begin{pmatrix}\widehat{\boldsymbol{B}}\\\widehat{\boldsymbol{B}'}\end{pmatrix}$ and $\widetilde{\boldsymbol{C}} \equiv (\boldsymbol{C}\ \boldsymbol{C}')$. From $\widetilde{\boldsymbol{C}}$, only columns related to k-components are extracted and denoted as $\boldsymbol{C}_k$, i.e. $\boldsymbol{C}_k \equiv (\boldsymbol{C}_{:k}\ \boldsymbol{C}_{:k}\odot\boldsymbol{C}_{:1}\ \boldsymbol{C}_{:k}\odot\boldsymbol{C}_{:2} \dots \boldsymbol{C}_{:k}\odot\boldsymbol{C}_{:K}) \in \mathbb{R}_+^{N\times K}$. In the same manner, k-component related rows of $\widetilde{\boldsymbol{B}}$ are extracted and denoted as $\boldsymbol{B}_k$. Using $\boldsymbol{C}_k$ and $\boldsymbol{B}_k$, the objective function can be written as: $L = \frac{1}{2}\|\boldsymbol{A}_k - \boldsymbol{C}_k\boldsymbol{B}_k\|_F^2$, where $\boldsymbol{A}_k \equiv \widehat{\boldsymbol{A}} - \widetilde{\boldsymbol{C}}\widetilde{\boldsymbol{B}} + \boldsymbol{C}_k\boldsymbol{B}_k$. The gradient of C_{nk} with to objective function is computed as follows:

$$\frac{\partial L}{\partial C_{nk}} = Tr\left[\frac{\partial \boldsymbol{C}_k}{\partial C_{nk}}\left(\frac{\partial L}{\partial \boldsymbol{C}_k}\right)^T\right] \qquad (6)$$

The nth row of $\frac{\partial \boldsymbol{C}_k}{\partial C_{nk}}$ can be calculated as $(1\ C_{n1}\ C_{n2} \dots C_{nk}) \equiv \boldsymbol{c}^{\prime k^T}$ and all the other rows are zeros. Therefore, Eq. 6 can be calculated as follows:

$$\frac{\partial L}{\partial C_{nk}} = {c'}^{k^T}\left[B_k B_k^{\ T} C_k^{\ T} - B_k A_k^{\ T}\right]_{:n}$$

The optimized C_{nk} can be obtained by setting $\frac{\partial L}{\partial C_{nk}} \equiv 0$ and calculated as:

$$C_{nk} = \frac{{c'}^{k^T} B_k \left(A_k^{\ T}\right)_{:n}}{{c'}^{k^T} B_k B_k^{\ T} c'^{k}} \tag{7}$$

If C_{nk} becomes negative values, then C_{nk} is set to zero.

Once $\widehat{B}^{(t)}$ and $C^{(t)}$ are updated, $\widehat{B}'$ can be immediately updated using generalized least absolute shrinkage of selection operators (LASSO) algorithm.[6] This problem is formulated as follows with temporally fixed $\widehat{B}^{(t)}$ and $C^{(t)}$:

$$\min_{\widehat{B'}} \frac{1}{2}\left\|\bar{A} - C'\widehat{B'}\right\|_F^2 + \rho\|B'\|_1, \tag{8}$$

$$s.t. \widehat{B'} = B'L$$

where $\bar{A} \equiv \widehat{A} - C\widehat{B}$. The NL-RQMS cyclically updating $\widehat{B}$, C and $\widehat{B}'$ is outlined as follows.

Algorithm 1: Pseudo-code for NL-RQMS

Input: sample-wise FA: $A \in \mathbb{R}_+^{N \times M}$, fragment spectra: $S \in \mathbb{R}_+^{M \times D}$, the number of system constituents: K, regularization parameters: (α, β, ρ)

Output: fraction: $C \in \mathbb{R}_+^{N \times K}$, FAs of the constituents: $B \in \mathbb{R}_+^{K \times M}$, FAs of cross-component: $B' \in \mathbb{R}_+^{K' \times M}$

Initialization

calculate L via Cholesky decomposition of SS^T

set $\widehat{A} = AL$

initialize $\widehat{B}$ and C using linear RQMS algorithm.

Repeat until convergence criteria is satisfied:

Calculate $\bar{A} = \hat{A} - C\hat{B}$.

Calculate C' following Eq. 4.

update $\widehat{B'}$ by solving Eq. 8 using generalized LASSO.

Calculate $\widehat{A'} = \hat{A} - C'\widehat{B'}$.

Update $\hat{B} = volmin(\widehat{A'}; C)$

Update C by Eq. 7.

Normalize C so that sum-to-one constraint is satisfied.

return C, B and B'

Supplementary Figures and Tables
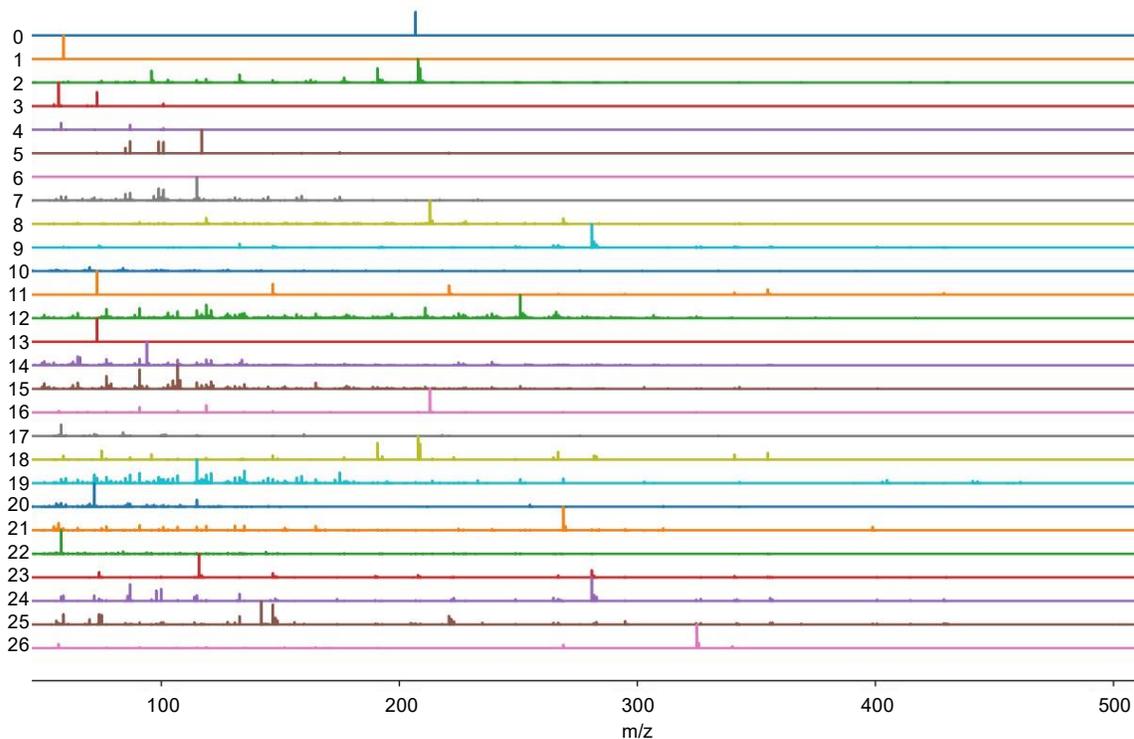
Fig. S1. The extracted 27–fragment spectra (**S**) from the spectral dataset **X** containing 310 spectra (31 samples × 10 temperature bands). The fragment abundances (FAs) of these 27 spectra in each sample is numerically presented in Table S1 and depicted as a heatmap in Fig. 2A.
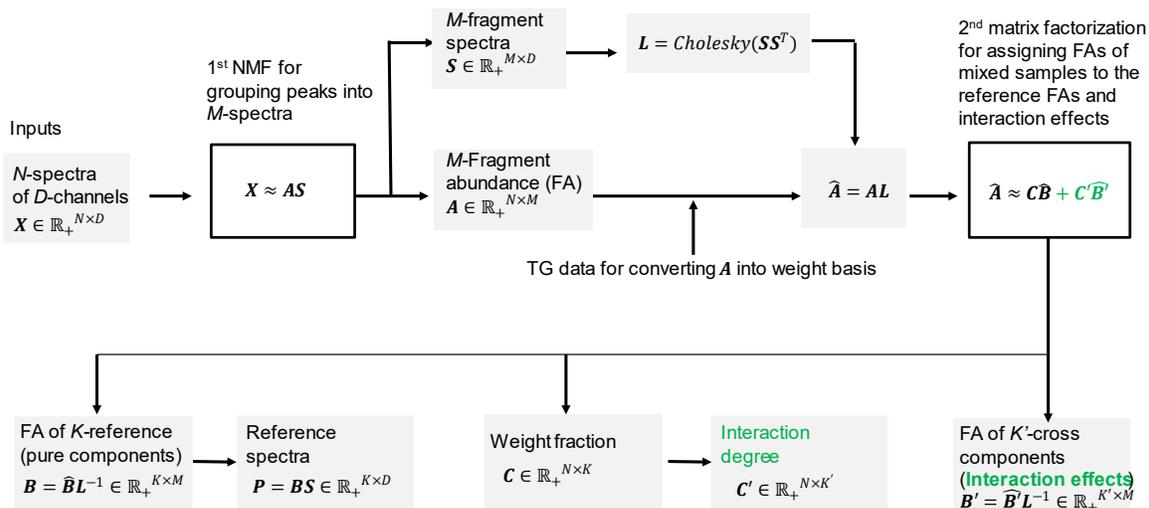
Fig. S2. (NL-)RQMS flowchart and definition of terminologies. Channels: *m/z* positions of centroid peaks; fragment spectra: groups of peaks whose intensities fluctuates at a certain ratio across the entire spectral dataset; fragment abundance (FA): the abundances of the fragment spectra in each sample; reference: a pure system component; cross-component: the interaction effects caused by mixing two references, influencing the FAs in mixed samples. The incorporation of thermogravimetry data for converting FA to a weight basis is detailed in the previous report.[1]
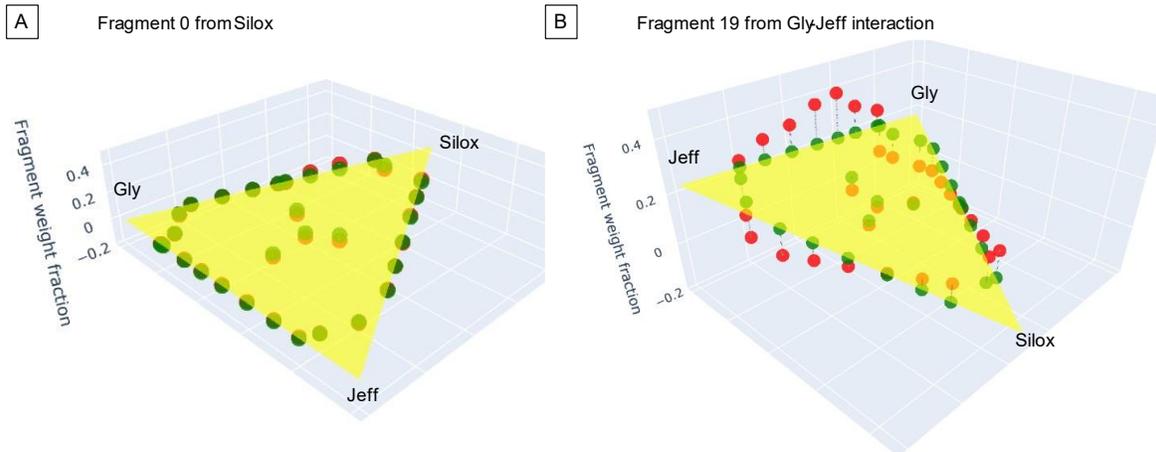
Fig. S3. Estimating the nonlinearity effect on fragment abundance (FA). Red points represent the measured FA for each sample, while the yellow triangular plane is the best-fit plane that these red points align with. Green points mark where perpendicular lines from red dots intersect with the plane. Nonlinearity is evaluated by the deviation from the plane. (A) FA of a non-interacting fragment derived from Silox, where the plane slopes towards the Silox vertex, indicating that most sample FAs are close to the best-fit plane. (B) FA of fragment 19, which results from Gly-Jeff interactions, shows that most points deviate from the plane. Since the true Gly, Jeff, and Silox samples contain almost no fragment 19 (Fig. 2A), the actual plane should be near FA = 0 plane. This suggests that using a linear analysis to estimate the plane for such nonlinear data leads to significant errors. The weight fraction of fragments caused by nonlinear interactions in this dataset is calculated by dividing the total distance of data points from the plane by the number of samples, showing that 41% of the total weight is influenced by nonlinear effects.
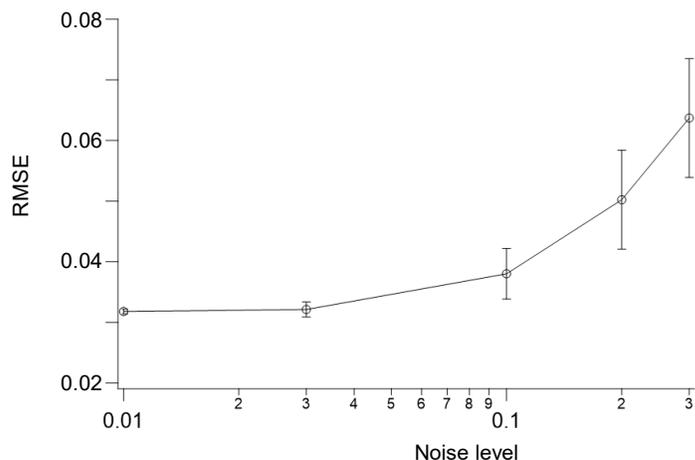
Fig. S4. Testing Robustness Against Noise in Input Data. The sample variance for each fragment in the input FA matrix data was calculated, and Gaussian noise, with a variance between 1% and 30% of the sample variance, was randomly added to the input data. Noise was introduced ten times for each noise level, and the error from the true composition was measured as the RMSE of the estimated composition values. The average RMSE was plotted against the noise levels, with error bars showing the standard deviation across the ten trials. The results indicate that estimation accuracy remains stable up to noise levels of around 10%, demonstrating the robustness of NL-RQMS in handling noise.

(Obsd. 251.107, Calcd. 251.107)

(Obsd. 207.033, Calcd. 207.033)

(Obsd. 115.076, Calcd. 115.076)

(Obsd. 72.081, Calcd. 72.081)

(Obsd. 325.144, Calcd. 325.144)

Fig. S5. Characterization of important fragment spectra identified as having positive or negative nonlinear effects by NL-RQMS analysis. The observed and calculated masses were highly consistent.

Table S1.

The hyper parameters of the first NMF $X \approx AS$ and the second factorization $A \approx CB + C'B'$.

Dataset	Sample number N	First NMF to calculate FA				Second factorization			
		w_o	Merging threshold	Initial M	iteration	K	$\alpha = \beta$	p	ρ
Gly/Jeff/Silox	31	0.2	0.99	30	3000	3	0.1	1.5	0.03

w_o: This parameter defines the strictness of orthogonality. A higher wo value indicates fewer shared peaks among the fragment spectra. The value of w_o should range between 0 and 1, where 0 implies no orthogonality constraint and 1 represents the strictest constraint.

Merging threshold and initial M: These parameters are associated with the automatic relevance determination (ARD) mechanism. The initial number of bases should be set larger than the appropriate number, and the ARD mechanism reduces the number of basis spectra by merging them when the cosine similarity of spectra exceeds the "merging threshold."

K: The number of system constituents.

α: The regularization hyperparameter that controls the minimum volume constraint for the simplex spanned by the reference spectra. A higher α value results in a more contracted simplex.

β: The regularization hyperparameter that controls the orthogonality among the reference spectra. A higher β value leads to a more expanded simplex.

p: The hyperparameter that controls robustness against outliers, which should be specified between 0.5 and 2. A higher p makes the second factorization more sensitive to data variation but less robust to outliers.

ρ: This parameter controls the sparseness of the interaction term of B'.

Table S2.

FileNames	Known composition			Inferred composition (linear)			Inferred composition (nonlinear)		
	Gly	Jeff	Silox	Gly	Jeff	Silox	Gly	Jeff	Silox
gly10jeff10silox80	0.15	0.05	0.80	0.11	0.01	0.89	0.13	0.06	0.81
gly10jeff80silox10	0.05	0.80	0.15	0.00	0.79	0.21	0.07	0.75	0.18
gly10jeff80silox10	0.15	0.80	0.05	0.09	0.83	0.07	0.15	0.75	0.10
gly20jeff40silox40	0.21	0.39	0.40	0.20	0.37	0.43	0.25	0.38	0.38
gly20jeff80	**0.20**	**0.80**	**0.00**	**0.15**	**0.85**	**0.00**	**0.21**	**0.79**	**0.00**
gly20silox80	0.20	0.00	0.80	0.17	0.00	0.83	0.19	0.00	0.81
gly30jeff70	**0.29**	**0.71**	**0.00**	**0.23**	**0.77**	**0.00**	**0.29**	**0.71**	**0.00**
gly30silox70	0.32	0.00	0.68	0.23	0.00	0.77	0.27	0.00	0.73
gly33jeff33silox33	0.33	0.33	0.34	0.29	0.32	0.38	0.34	0.31	0.34
gly40jeff20silox40	0.40	0.20	0.41	0.35	0.20	0.45	0.40	0.20	0.39
gly40jeff40silox20	0.40	0.40	0.20	0.37	0.43	0.20	0.41	0.38	0.20
gly40jeff60	**0.40**	**0.60**	**0.00**	**0.29**	**0.71**	**0.00**	**0.38**	**0.62**	**0.00**
gly40silox60	0.41	0.00	0.59	0.36	0.00	0.64	0.42	0.00	0.58
gly50jeff50	**0.51**	**0.49**	**0.00**	**0.39**	**0.61**	**0.00**	**0.51**	**0.49**	**0.00**
gly50silox50	0.50	0.00	0.51	0.45	0.00	0.55	0.52	0.00	0.48
gly50silox50	0.52	0.00	0.48	0.44	0.00	0.56	0.52	0.00	0.48
gly60jeff40	**0.60**	**0.40**	**0.00**	**0.43**	**0.57**	**0.00**	**0.58**	**0.42**	**0.00**
gly60silox40	0.60	0.00	0.40	0.55	0.00	0.45	0.62	0.00	0.38
gly70jeff30	**0.68**	**0.32**	**0.00**	**0.49**	**0.51**	**0.00**	**0.62**	**0.38**	**0.00**
gly70silox30	0.70	0.00	0.30	0.69	0.00	0.31	0.75	0.00	0.25
gly80jeff10silox10	0.81	0.04	0.14	0.88	0.01	0.11	0.86	0.03	0.11
gly80jeff10silox10	0.78	0.16	0.07	0.80	0.20	0.00	0.83	0.14	0.03
gly80jeff20	**0.79**	**0.21**	**0.00**	**0.62**	**0.38**	**0.00**	**0.74**	**0.26**	**0.00**
gly80jeff20	0.80	0.20	0.00	0.70	0.30	0.00	0.71	0.28	0.02
gly80silox20	0.80	0.00	0.20	0.83	0.00	0.17	0.87	0.00	0.13
jeff20silox80	0.00	0.21	0.79	0.00	0.15	0.85	0.00	0.23	0.77
jeff30silox70	0.00	0.29	0.71	0.00	0.24	0.76	0.00	0.33	0.67
jeff40silox60	0.00	0.39	0.61	0.00	0.35	0.65	0.00	0.45	0.55
jeff50silox50	0.00	0.51	0.49	0.00	0.49	0.51	0.00	0.58	0.42
jeff60silox40	0.00	0.61	0.39	0.00	0.57	0.43	0.00	0.66	0.34
jeff70silox30	0.00	0.71	0.30	0.00	0.66	0.34	0.00	0.74	0.26

The precisions of linear and nonlinear RQMS were assessed by calculating the root mean squared error (RMSE) of C in comparison to the ground truth $\overline{C}$, i.e., $RMSE = \sqrt{\frac{1}{N}\sum_k^K \sum_n^N (C - \overline{C})_{kn}^2}$, where N is the dataset seize ($N=31$) and K is the number of the system component ($K = 3$). Data points on the Gly-Jeff edge are bolded to highlight the significant

improvement in estimation accuracy achieved by updating to nonlinear RQMS.

Data S1.

Numerical data of Fig. 2A. The values represent the 27–fragment abundances (weight fraction) in each sample, derived by reported algorithm using hyperparameters of Table S1.

Reference

(1)　Hibi, Y.; Uesaka, S.; Naito, M. Thermogravimetry-Synchronized, Reference-Free Quantitative Mass Spectrometry for Accurate Compositional Analysis of Polymer Systems Without Prior Knowledge of Constituents. *Analyst* **2024**. https://doi.org/10.1039/D4AN00624K.

(2)　Hibi, Y.; Uesaka, S.; Naito, M. A Data-Driven Sequencer That Unveils Latent "Codons" in Synthetic Copolymers. *Chem Sci* **2023**. https://doi.org/10.1039/d2sc06974a.

(3)　Fu, X.; Huang, K.; Yang, B.; Ma, W. K.; Sidiropoulos, N. D. Robust Volume Minimization-Based Matrix Factorization for Remote Sensing and Document Clustering. *IEEE Trans. Signal Process.* **2016**, *64* (23), 6254–6268. https://doi.org/10.1109/TSP.2016.2602800.

(4)　Heinz, D. C.; Chang, C.-I. Fully Constrained Least Squares Linear Spectral Mixture Analysis Method for Material Quantification in Hyperspectral Imagery. *IEEE Trans. Geosci. Remote Sens.* **2001**, *39* (3), 529–545.

(5)　Févotte, C.; Dobigeon, N. Nonlinear Hyperspectral Unmixing with Robust Nonnegative Matrix Factorization. *IEEE Trans. Image Process.* **2015**, *24* (12), 4810–4819. https://doi.org/10.1109/TIP.2015.2468177.

(6)　Roth, V. The Generalized LASSO. *IEEE Trans. Neural Netw.* **2004**, *15* (1), 16–28. https://doi.org/10.1109/TNN.2003.809398.